NAVAL POSTGRADUATE SCHOOL
Monterey, California

THESIS

DESIGN OF A TOROIDAL THERMOACOUSTIC PRIME MOVER

by

Yang, Szu-Wei

June 1995

Thesis Advisor: Anthony A. Atchley
Thesis Co-Advisor: Thomas J. Hofler

Approved for public release; distribution is unlimited

REPORT DOCUMENTATION PAGE

Form Approved
OMB No. 0704

1. AGENCY USE ONLY *(Leave blank)*	2. REPORT DATE	3. REPORT TYPE AND DATES COVERED
	June 1995	Master's Thesis

4. TITLE AND SUBTITLE
DESIGN OF A TOROIDAL THERMOACOUSTIC PRIME MOVER

5. FUNDING NUMBERS

6. AUTHOR(S)
Yang, Szu-Wei

7. PERFORMING ORGANIZATION NAME(S) AND ADDRESS(ES)
Naval Postgraduate School
Monterey CA 93943-5000

8. PERFORMING ORGANIZATION REPORT NUMBER

9. SPONSORING/MONITORING AGENCY NAME(S) AND ADDRESS(ES)

10. SPONSORING/MONITORING AGENCY REPORT NUMBER

11. SUPPLEMENTARY NOTES
The views expressed in this thesis are those of the author and do not reflect the official policy or position of the Department of Defense or the U.S. Government.

12a. DISTRIBUTION/AVAILABILITY STATEMENT
Approved for public release;
Distribution unlimited.

12b. DISTRIBUTION CODE

13. ABSTRACT *(maximum 200 words)*

The topic of this thesis is the design of a toroidal prime mover. The primary design tool is a MATLAB program based on a standing wave analysis of thermoacoustics. A conventional prime mover that has been well studied, was used for validating the program. DeltaE, a program developed at Los Alamos National Laboratory for designing thermoacoustic engines, was also used as an auxiliary tool for validation test purposes. The validation suggested that the MATLAB program models the onset conditions of a conventional prime mover with fair accuracy. The program was then applied to a toroidal prime mover. A series of analyses were conducted on a toroidal prime mover to determine the influence of prime mover circumference, stack length, and duct radius. The final design calls for a 150 cm circumference, 2.54 cm duct radius, and 1.9 cm stack length. The contributions of this thesis are: (1) to develop and validate the MATLAB simulation program; (2) to provide a draft design for a toroidal prime mover for future research.

14. SUBJECT TERMS	15. NUMBER OF PAGES
Thermoacoustics; Thermoacoustic Heat Transport; Prime Mover; Toroidal Prime Mover	62
	16. PRICE CODE

17. SECURITY CLASSIFICATION OF REPORT	18. SECURITY CLASSIFICATION OF THIS PAGE	19. SECURITY CLASSIFICATION OF ABSTRACT	20. LIMITATION OF ABSTRACT
Unclassified	Unclassified	Unclassified	UL

NSN 7540-01-280-5500

Standard Form 298 (Rev. 2-89)
Prescribed by ANSI Std. 239-18

Approved for public release; distribution is unlimited.

DESIGN OF A TOROIDAL THERMOACOUSTIC PRIME MOVER

Yang, Szu-Wei
Lieutenant Commander, Taiwan Navy
B.S., Chinese Naval Academy, 1983

Submitted in partial fulfillment
of the requirements for the degree of

MASTER OF SCIENCE IN ENGINEERING ACOUSTICS

from the

NAVAL POSTGRADUATE SCHOOL
June 1995

Author: 楊思偉 Yang, Szu-Wei
Yang, Szu-Wei

Approved by: Anthony A. Atchley
Anthony A. Atchley, Thesis Advisor

Thomas J. Hofler
Thomas J. Hofler, Thesis Co-Advisor

Anthony A. Atchley
Anthony A. Atchley
Chairman, Engineering Acoustics Academic Committee

ABSTRACT

The topic of this thesis is the design of a toroidal prime mover. The primary design tool is a MATLAB program based on a standing wave analysis of thermoacoustics. A conventional prime mover that has been well studied, was used for validating the program. DeltaE, a program developed at Los Alamos National Laboratory for designing thermoacoustic engines, was also used as an auxiliary tool for validation test purposes. The validation suggested that the MATLAB program models the onset conditions of a conventional prime mover with fair accuracy. The program was then applied to a toroidal prime mover. A series of analyses were conducted on a toroidal prime mover to determine the influence of prime mover circumference, stack length, and duct radius. The final design calls for a 150 cm circumference, 2.54 cm duct radius, and 1.9 cm stack length. The contributions of this thesis are: (1) to develop and validate the MATLAB simulation program; (2) to provide a draft design for a toroidal prime mover for future research.

TABLE OF CONTENTS

LIST OF SYMBOLS

a	sound speed
c_p	isobaric heat capacity per unit mass
E	dissipated acoustic power
E_{st}	stored energy
ω	angular frequency
Q	quality factor
W	generated acoustic power
p	acoustic pressure
p_1	acoustic pressure amplitude
P_A	peak acoustic pressure amplitude
u	acoustic particle velocity
u_1	acoustic velocity amplitude
ρ_m	mean gas density
l	plate half-thickness
y_0	plate half-spacing
ϕ	phase angle
R	resonator
S	cross sectional area of fluid
k	propagation constant
K	thermal conductivity
t	time
T_m	mean temperature
γ	ratio of specific heat
μ	dynamic viscosity
σ	Prandtl number
ε_s	plate heat capacity ratio
x	direction along sound propagation
y	direction perpendicular to sound propagation
δ_s	thermal penetration depth in the solid plate

δ_t thermal penetration depth in the gas

δ_v viscous penetration depth in the gas

ACKNOWLEDGEMENT

I would like to express my sincere appreciation to my advisors, Dr. Anthony A. Atchley and Dr. Thomas J. Hofler for their assistance and instruction while working my thesis. Also, I would like to thank my parents for supporting and encouraging me through the whole two years and four months of study here.

I. INTRODUCTION

There have been many NPS theses involving several aspects of thermoacoustic heat transport. One area of particular concentration has been thermoacoustic prime movers [See Refs. 1-3, for example]. A thermoacoustic prime mover is a class of thermoacoustic heat engine that converts thermal energy into useful work in the form of sound. The purpose of this thesis is to explore the design of a toroidal prime mover.

A typical prime mover configuration is illustrated in Fig. 1. During operation, a temperature difference is imposed between the two heat exchangers, resulting in a temperature gradient in the stack. (The terms hot and cold are used to indicate that there is a temperature difference between these regions of the prime mover. They are not meant to imply anything about the absolute temperature involved). When the gradient is sufficiently high, acoustic oscillations spontaneously build up in the prime mover. At this point the prime mover is said to have reached onset. The conditions necessary for a prime mover to reach onset are typically discussed in terms of which of two quantities is greater: the thermoacoustic gain of the stack, or the dissipation due to thermo-viscous wall losses and power delivery to an external load. The importance of each of these factors is determined by the geometry of the prime mover, e.g., where the stack is located relative to the nearest acoustic pressure antinode, *etc*. The positions of the components of a prime mover relative to the acoustic field are usually fixed by incorporating well defined acoustic boundary conditions into the design of the engine. For instance, placement of a rigid boundary in the engine insures that the acoustic velocity is zero at that point. These "built-in" boundary conditions serve as convenient starting points for computational analysis of the performance of an engine.

A frequently asked question, when explaining how a prime mover generates sound (once the temperature gradient in the stack is sufficiently high) is "What is the origin of the low amplitude sound that gets amplified by the prime mover?" When answering, one usually resorts to postulation the existence of fluctuations or noise having a component with the right frequency and acoustic phase to be amplified by the stack.

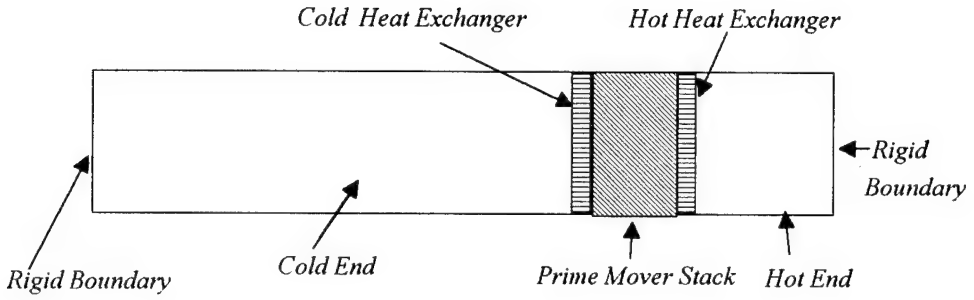

Figure 1 - A typical prime mover configuration

In light of this discussion, a toroidal prime mover poses some interesting questions. As shown in Fig. 2, a toroidal prime mover has the cold end connected to the hot end via a duct that does not impose, at first glance, any obvious dominating boundary conditions that would force an antinode at any particular point. Indeed, if the stack and heat exchangers were not there and if the toroid had a uniform cross section, a standing wave should have no preferential orientation. In other words, there is no place that one knows *a priori* is going to be a pressure antinode, for example. However, one might argue that even with periodic boundary conditions, fluctuations still exist and there will be a component that matches the conditions necessary for amplification.

Assuming that a toroidal prime mover can go into onset, a number of interesting questions arise. Will the standing wave (if it is an standing wave) adjust its spatial orientation to optimize the thermoacoustic gain? In other words, will the prime mover put the stack where it wants, where its performance is optimized? A rigid ended prime mover does not offer this possibility of self-optimization. Will deviations in measured stack locations from those predicted be indicative of unaccounted for processes such as acoustic streaming or turbulence? Another interesting question concerns multimode excitation. It has been previously shown that two modes can be excited in a prime mover simultaneously [Refs. 3 and 4]. However, due to the presence of rigid boundaries, the stack placement is optimized for only one mode. A toroidal geometry with periodic boundary conditions offers the possibility that each mode could optimize itself.

All these questions presuppose that the prime mover will go into onset. The presence of the stack will break the ambiguity of the standing wave's spatial orientation. The stack has the highest flow impedance in the toroid. Because this impedance will tend to favor low acoustic velocities, the perturbation due to the presence of the stack might force a velocity node at the stack. This condition would necessarily make any thermoacoustic gain zero, preventing the prime mover from ever going into onset. Further, the fundamental mode of a uniform cross section toroid (one without a stack), corresponds to the circumference being equal to one acoustic wavelength. There are two orthogonal degenerate modes that satisfy this condition. The presence of a nonuniformity will break this degeneracy. One mode will have a velocity node at the stack, the other will

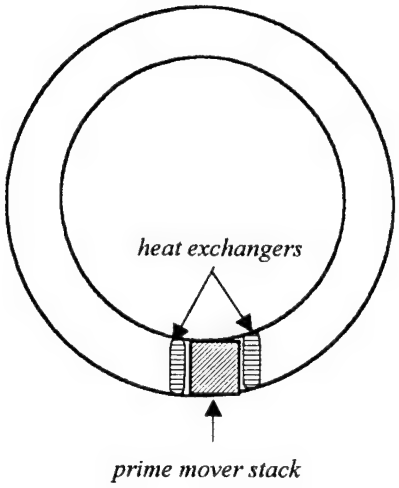

Figure 2 - Toroidal prime mover configuration

have a pressure node at the stack. Neither of these modes will be supported by thermoacoustics, but linear combinations would be supported. Other nonuniformities in cross section, will also have an effect on the spatial distribution of the acoustic variables. Hence, by placing a constriction or expansion in the toroid, the previously mentioned velocity and pressure nodes will be displaced from the stack, allowing for the possibility of thermoacoustic gain.

This discussion leads one to conclude that designing a functioning toroidal prime mover may be considerably more difficult than designing a conventional prime mover. The research described in this thesis addresses only the first part of the problem. That problem is to design a toroidal prime mover that, presupposing onset is possible, should reach onset at a temperature difference that is easily attainable in the laboratory.

The approach taken is to use a simple formulation of the basic equations for thermoacoustics to predict the onset conditions for a toroidal prime mover. The program developed around this formulation will first be validated by comparing its predictions to data taken previously on a rigid ended prime mover [Ref. 1]. The predicted onset conditions will also be compared to those determined using DeltaE, a program developed at Los Alamos National Laboratory for designing thermoacoustic engines. After validation, the MATLAB program will be used to design a toroidal prime mover.

Chapter II contains a brief review of the theory pertinent for this work. The validation of the program is discussed in Chapter III. Some experiments with a toroidal prime mover are presented in Chapter IV. An improved design is presented in Chapter V.

II. THEORY

It has been shown previously that tracking the quality factor (Q) of a prime mover as a function of temperature difference across the stack is a convenient way to predict onset. This chapter contains a discussion of how to calculate the Q of a prime mover as a function of the applied temperature difference. The discussion is based on a standing wave analysis described in detail in Ref. 5 and draws heavily upon the derivation presented there.

In addition, brief descriptions of the two different computer programs, one written in MATLAB [Ref. 6] by the author, and DeltaE [Ref. 7] will be given at the end of this chapter.

A. STANDING WAVE ANALYSIS OF A THERMOACOUSTIC PRIME MOVER

The derivation begins by making the connection between the power output of a prime mover and quality factor. Next, an expression is derived for the power output of a prime mover stack. Following this derivation, the thermal and viscous losses in the remainder of the prime mover are discussed. Finally, an expression is derived for the energy stored in the prime mover.

1. Relationship Between Power Output And Quality Factor

The reciprocal of the quality factor of a prime mover below onset can be expressed as

$$1/Q = -\dot{W}/\omega E_{ST} \tag{1}$$

The net power output $\dot{W}$ is the sum of the power output of the individual sections of the prime mover :

$$\dot{W}=\dot{W}_{hot}+\dot{W}_{hot\,hx}+\dot{W}_{pms}+\dot{W}_{cold\,hx}+\dot{W}_{cold}\,. \tag{2}$$

The subscripts hot, hot hx, pms, cold hx, and cold refer to the hot end, the hot heat

exchanger, the prime mover stack, the cold heat exchanger and the cold end, respectively. E_{ST} is the acoustic energy stored in the prime mover. w is the angular frequency of the acoustic oscillation. At onset $\dot{W}=0$, so $1/Q=0$. $\dot{W}=0$ means that the power output of the stack exactly cancels the losses elsewhere in the prime mover, so the net power output is zero.

2. Acoustic Power Output Of The Prime Mover Stack

In Eq. (1) $\dot{W}_{pms}$ is the power output of the stack. In general, $\dot{W}_{pms} = \int_{x1}^{x2} d\dot{W}_{pms}$, where $d\dot{W}_{pms}$ is the differential power output of a segment of the stack located between x and $x+dx$. It is found by taking the difference in the acoustic intensity at the two ends of the segment and multiplying the result by the cross-sectional area of the fluid in the stack S_{pms} (the x direction is along the resonator axis, the direction of sound propagation).

$$d\dot{W}_{pms} = S_{pms}[\langle\overline{pu}\rangle_{x+dx} - \langle\overline{pu}\rangle_x]. \tag{3}$$

The overbar indicates time average and the brackets $\langle\rangle$ indicate average in the y direction. (The y direction is perpendicular to the resonator axis and the plate surface.) The stack plates are $2l$ thick and spaced by $2y_0$. Expanding $\langle\overline{pu}\rangle_{x+dx}$ and assuming that p is independent of y, Eq. (3) can be written as

$$d\dot{W}_{pms} = S_{pms}\frac{d\overline{p\langle u\rangle}}{dx}dx. \tag{4}$$

The acoustic variables can be expressed as $p = p_1 e^{jwt}$ and $u = u_1 e^{jwt}$, where

$$p_1 = P_A \cos[\phi(x)], \tag{5}$$

and

$$\langle u_1\rangle = -j\frac{P_A}{\rho_m a}\left(1+\frac{l}{y_0}\right)\sin[\phi(x)]. \tag{6}$$

In these equations, P_A is defined to be the peak acoustic pressure amplitude at the rigid end, at $x=0$. Changes in pressure amplitude due to changes in resonator cross section are neglected. Also, $\phi(x)$ represents the phase of the standing wave at the location of the segment. If the propagation constant k is independent of position, $\phi(x) = kx$. However, in general,

$$\phi(x) = \int_0^x k(\xi)d\xi \tag{7}$$

The term $(1 + l/y_0)$ arises from the requirement that volume velocity be conserved and the desire to relate the acoustic velocity in the stack to P_A.

The time average of the product of two complex quantities such as p and $\langle u \rangle$ is

$$\overline{p\langle u\rangle} = \tfrac{1}{2} Re[p_1 \langle \tilde{u}_1 \rangle] \tag{8}$$

(~ denotes complex conjugate), Eq. (4) becomes

$$d\dot{W}_{pms} = \tfrac{1}{2} S_{pms} Re(p_1 \frac{d\langle \tilde{u}_1 \rangle}{dx} + \frac{dp_1}{dx} \langle \tilde{u}_1 \rangle) dx \tag{9}$$

The expression for dp_1/dx and $d\langle \tilde{u}_1 \rangle/dx$, are obtained from Swift [Ref. 8]:

$$\frac{dp_1}{dx} = \frac{-j\omega\rho_m}{1 - f_v} \langle u_1 \rangle \tag{10}$$

and

$$\frac{d\langle u_1 \rangle}{dx} = \frac{j}{\omega\rho_m} \frac{f_k - f_v}{(1-\sigma)(1+\varepsilon_s)} \frac{\nabla T_m}{T_m} \frac{dp_1}{dx} - \frac{j}{\omega\rho_m} \frac{\omega^2}{a^2} \left(1 + \frac{\gamma - 1}{1 + \varepsilon_s} f_k\right) p_1. \tag{11}$$

The functions f_k, f_v and ε_s are given by

$$f_k = \frac{\tanh[(1+j)y_0/\delta_k]}{(1+j)y_0/\delta_k}, \tag{12}$$

$$f_v = \frac{\tanh[(1+j)y_0/\delta_v]}{(1+j)y_0/\delta_v}, \tag{13}$$

and

$$\varepsilon_s = \frac{\rho_m c_p \delta_k \tanh[(1+j)y_0/\delta_k]}{\rho_s c_s \delta_s \tanh[(1+j)l/\delta_s]}, \tag{14}$$

where the thermal and viscous penetration depths in the gas are defined as

$$\delta_k = \sqrt{2K/\rho_m c_p \omega}, \tag{15}$$

and

$$\delta_v = \sqrt{2\mu/\rho_m\omega}\,. \tag{16}$$

The definition of the thermal penetration depth in the solid plate δ_s is similar to that of δ_k. The Prandtl number σ is given by

$$\sigma = c_p\mu/K. \tag{17}$$

Substituting Eqs. (5), (6), (10), and (11) into Eq. (9) gives the power output of the element

$$d\dot{W}_{pms} = \frac{1}{2}S_{pms}Re\left\{\frac{P_A^2\omega}{\rho_m a^2}\left[j\left(\frac{\tilde{f}_k - \tilde{f}_v}{1-\tilde{f}_v}\frac{1+l/y_0}{(1-\sigma)(1+\varepsilon_s)}\frac{\nabla T_m}{kT_m}\tan\phi(x) + 1 + \frac{(\gamma-1)}{1+\varepsilon_s}\tilde{f}_k\right)\right.\right.$$

$$\left.\left.\times\cos^2(x) - j\frac{(1+l/y_0)^2}{1-f_v}\sin^2\phi(x)\right]\right\}dx. \tag{18}$$

The total acoustic power output of the stack is found by integrating Eq. (18) along the entire length of the stack.

3. Thermal and Viscous Losses In The Remainder of The Prime Mover

Thermal and viscous losses can be calculated from Eq. (18) with only slight modifications. The calculation is simplified by the absence of temperature gradients in the remainder of the prime mover, i.e. $\nabla T_m = 0$.

$$d\dot{W}_{hx} = \frac{1}{2}S_{hx}\,Re\left\{\frac{P_A^2\omega}{\rho_m a^2}j\left[\left(1 + \frac{(\gamma-1)\tilde{f}_k}{1+\varepsilon_s}\right)\cos^2\phi(x) - \frac{(1+l/y_0)^2}{1-f_v}\sin^2\phi(x)\right]\right\}dx. \tag{19}$$

Equation (19) also describes the losses in the cold end and hot end if l is set to zero and the appropriate form for S, f_k, and f_v are used. For a circular tube of radius R,

$$f_k = \frac{2J_1[(j-1)R/\delta_k]}{(j-1)(R/\delta_k)J_0[(j-1)R/\delta_k]}. \tag{20}$$

and

$$f_v = \frac{2J_1[(j-1)R/\delta_v]}{(j-1)(R/\delta_v)J_0[(j-1)R/\delta_v]}. \tag{21}$$

The thermal losses at the end caps are found by evaluating Eq. (19) at x=0 (the cold end) and x=L (the hot end) and replacing y_0 with L .

4. Stored energy

The energy stored in the prime mover is found by integrating the time-averaged acoustic energy density throughout the entire volume of the prime mover. The result is

$$E_{ST} = \frac{1}{4}\frac{P_A^2}{\rho_m a^2} S\{x_{cold} + \int_{coldhx}[\frac{\cos^2[\phi(x)]}{1+l/y_0} + (1+\frac{l}{y_0})\sin^2[\phi(x)]]dx$$

$$+\int_{pms}[\frac{\cos^2[\phi(x)]}{(1+l/y_0)} + (1+\frac{l}{y_0})\sin^2[\phi(x)]]dx$$

$$+\int_{hothx}[\frac{\cos^2[\phi(x)]}{(1+l/y_0)} + (1+\frac{l}{y_0})\sin^2[\phi(x)]]dx + x_{hot}\}, \tag{22}$$

where x_{cold} and x_{hot} refer to the length of the cold and hot end, respectively.

B. MATLAB PROGRAM

A MATLAB program was written to implement the standing wave analysis presented above to calculate $1/Q$ vs. ΔT. In regions where there is no gradient (everywhere except in the stack), integrals are evaluated analytically. A linear gradient is assumed in the stack. The stack is divided into 10 isothermal segments. The temperature-dependent thermal-physical parameters and acoustic phase are evaluated for each segment and the work output computed. The total work output of the stack is the sum of the work output of each segment. In rigid-ended prime movers, the position of the elements of the engine relative to the standing wave are determined by boundary conditions. In the toroidal prime mover, the location of the elements relative to the standing wave is an adjustable parameter.

C. DELTAE

DeltaE (Design Environment for Low Amplitude Thermoacoustic Engines) is a computer program written by Ward and Swift at Los Alamos National Laboratory [Ref.7]. It solves Rott's wave equation for a geometry defined by the user. More information on DeltaE can be found on internet at http://rott.esa.lanl.gov.

III. VALIDATION

The goal of this thesis is to design a toroidal thermoacoustic prime mover. As discussed in the previous chapter, the primary design tool is a MATLAB program based on the analysis presented in Ref. 5. The primary design goals are 1) to have an onset temperature difference that is easily reached experimentally and 2) to have dimensions that are practical from machining and experimental considerations.

The purpose of this chapter is to explain the process used to validate the MATLAB program. The program was validated in two ways. 1) It was used to predict the performance of Lin's prime mover below onset, a system that has been well studied previously. 2) Predictions of onset temperature difference (ΔT_{onset}) were compared to the predictions of DeltaE.

A. LIN'S PRIME MOVER

This prime mover, described in detail in Ref. 1 and Ref. 5, was used originally to investigate the low amplitude work output of a prime mover stack as a function of mean gas pressure and temperature difference across the prime mover stack. Figure 3 shows the prime mover configuration.

Both the heat exchangers and prime mover stack have parallel-plate geometry. The work output of this prime mover stack is modeled by Eq. (18) in Chapter II. The thermo-viscous losses in heat exchangers are modeled using Eq. (19). The losses in the cold and hot ends are calculated using Eq. (19). Equation (20) and (21) were used in the calculation instead of Eq. (12) and Eq. (13).

Figures 4 to 7 compare the MATLAB program results with the experimental results. The experimental data presented in these figures are composites of individual data sets recorded at different times. Figures 4 and 5 show how 1/Q changes with the ΔT for the prime mover filled with helium gas at a mean pressure of 376 kPa and 500 kPa. The computer simulation tends to underpredict the experimental onset values by about 20-30 degrees. Figures 6 and 7 show how resonance frequency changes with ΔT. The difference between simulation and experiment is less than 6 Hz, or approximately 1%. One known limitation of the standing wave analysis is that it ignores boundary layer effect

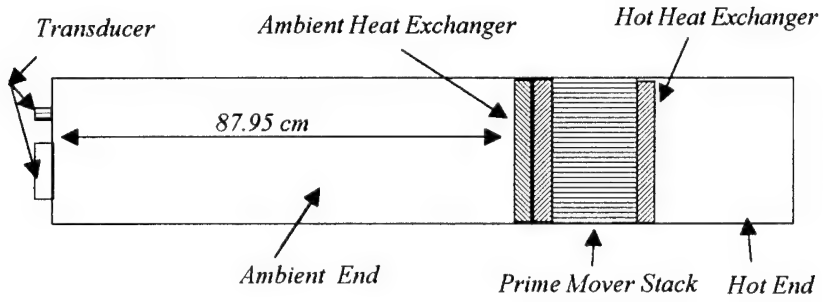

Figure 3 - Lin's prime mover configuration

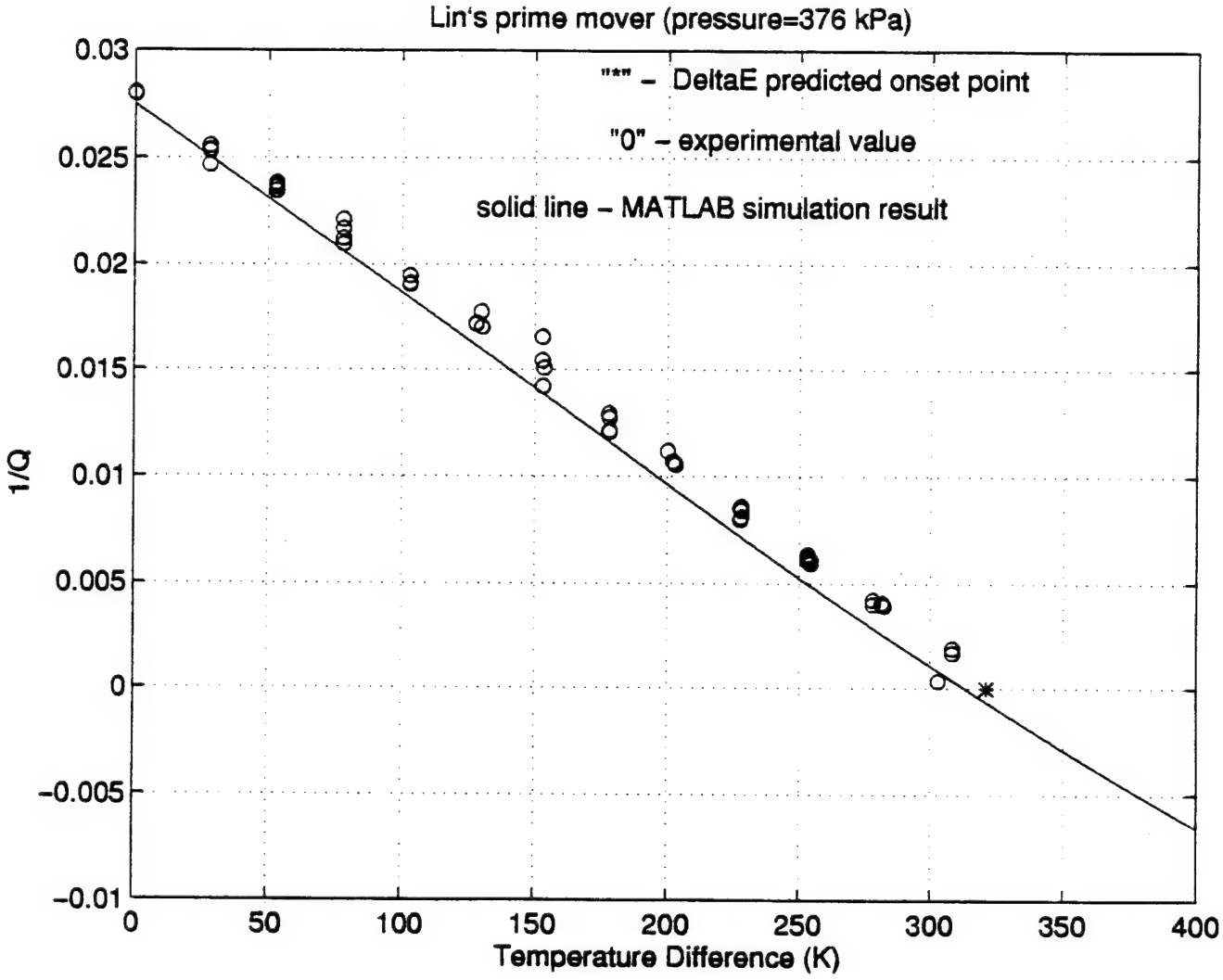

Figure 4 - Graph of 1/Q vs. ΔT for Lin's prime mover filled with helium gas at a mean pressure of 376 kPa.

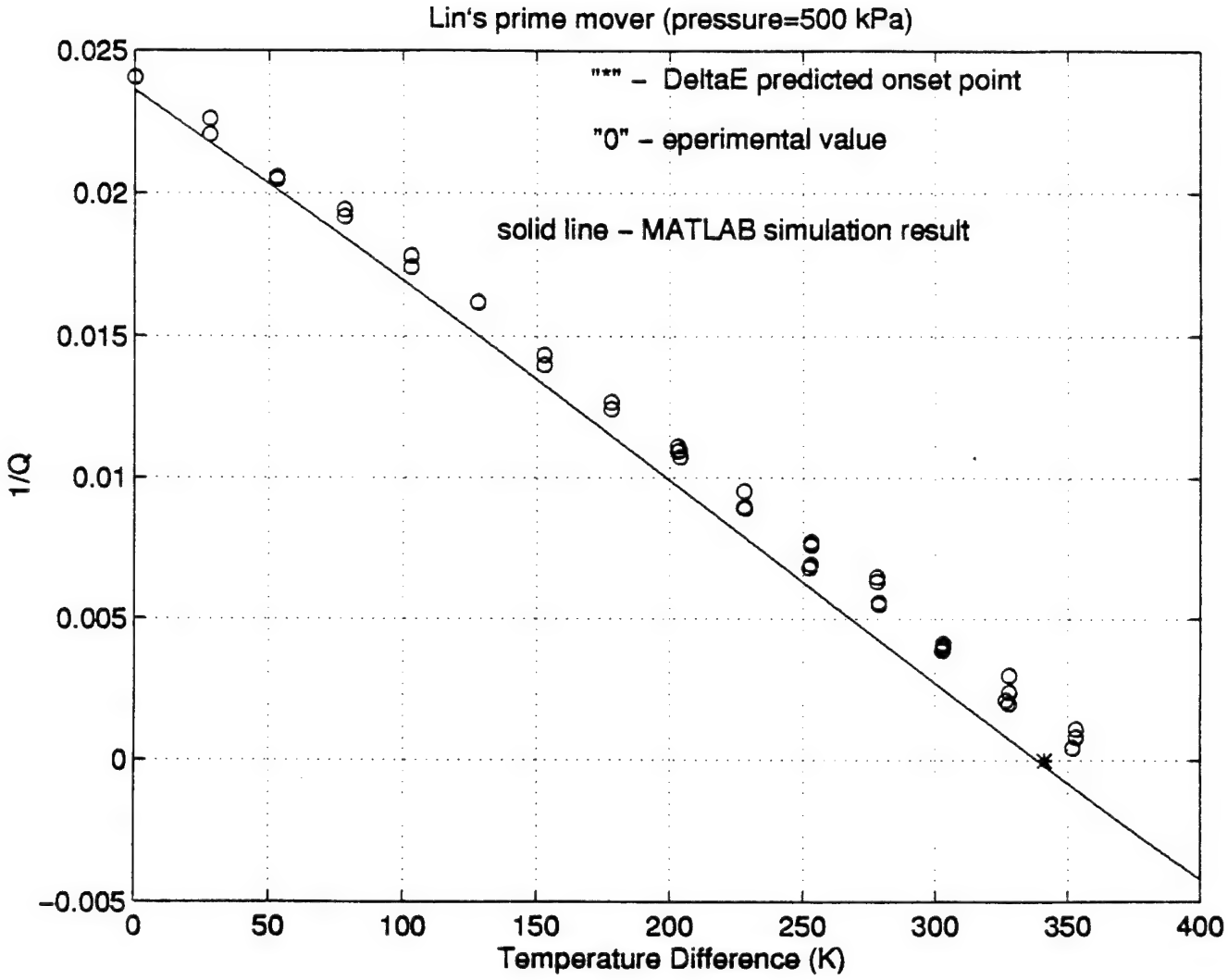

Figure 5 - Graph of 1/Q vs. ΔT for Lin's prime mover filled with helium gas at a mean pressure of 500 kPa.

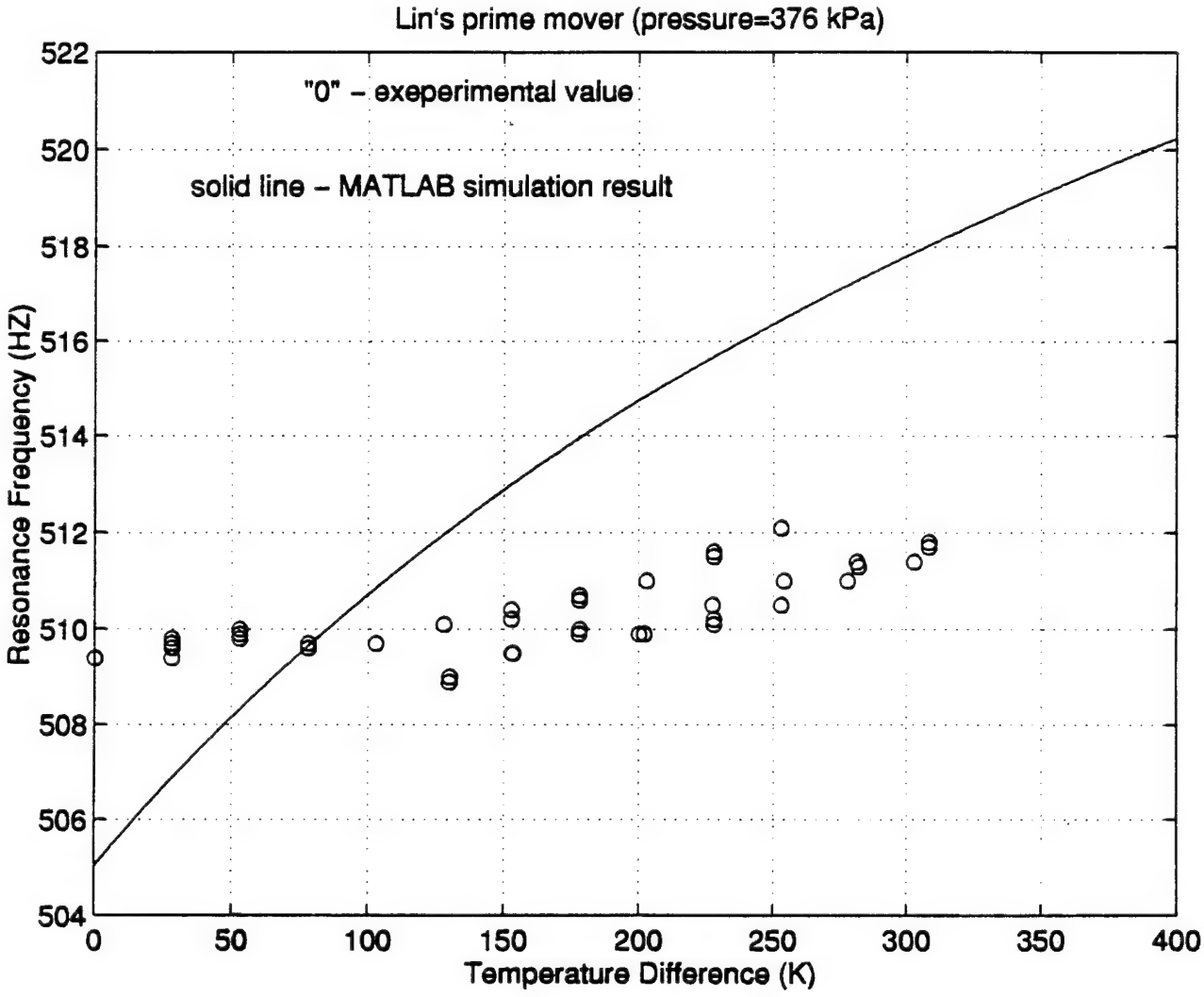

Figure 6 - Graph of resonance frequency vs. ΔT for Lin's prime mover filled with helium gas at a mean pressure of 376 kpa.

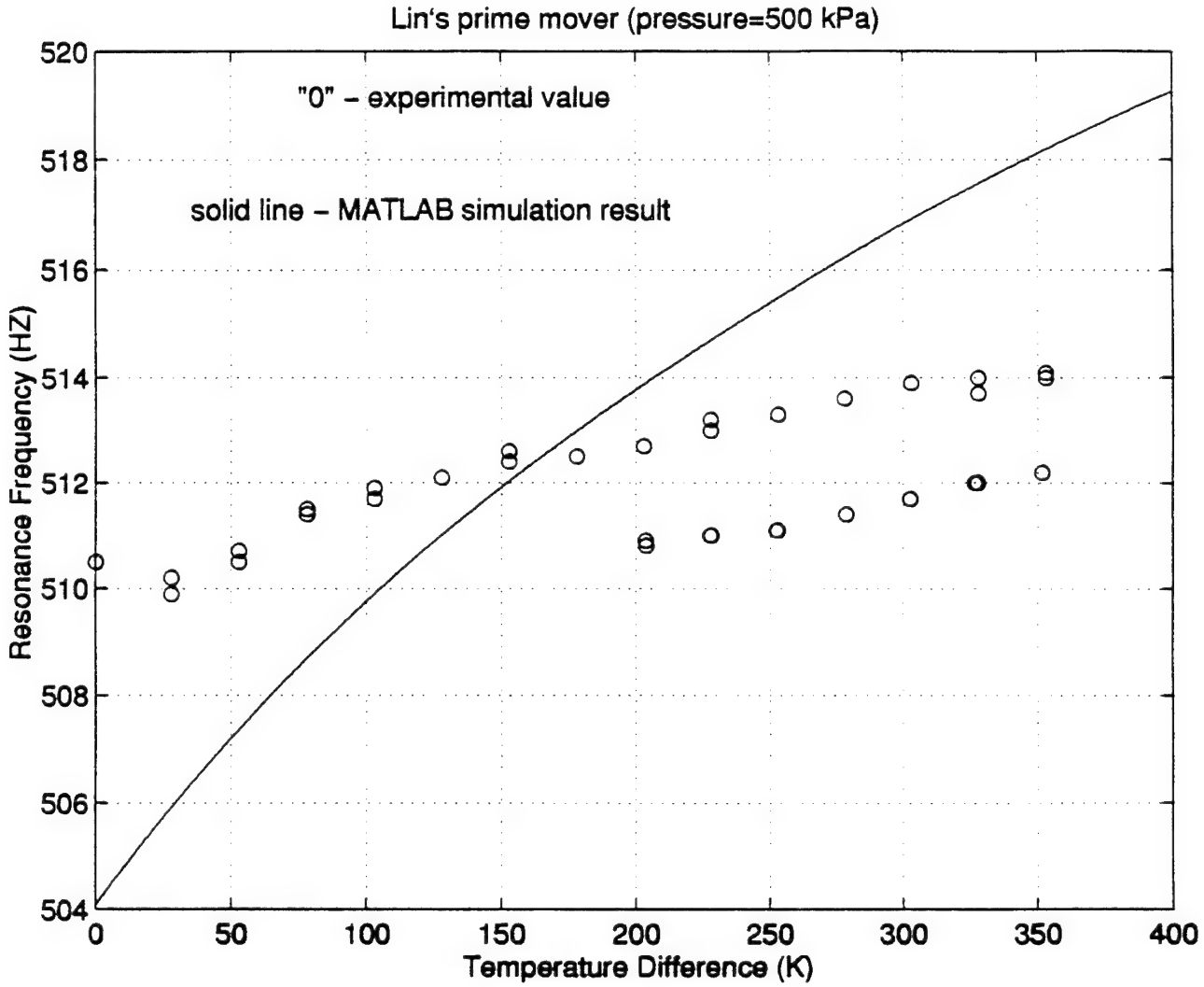

Figure 7 - Graph of resonance frequency vs. ΔT for Lin's prime mover filled with helium gas at a mean pressure of 500 kpa.

when calculating resonance frequency. However, the results are acceptable for the intended purpose.

B. DELTAE PROGRAM SIMULATION

The results of the DeltaE simulation of Lin's prime mover are shown in Figs. 8-10. The prime mover is filled with helium, at a mean pressure of 376 kpa. Figure 8 shows the heat input to hot heat exchanger as a function of the work output of the prime mover. Notice that there is a linear relationship. Extrapolation of a linear least squares fit to the points shows that the work output goes to zero at a heat input of approximately 44 W. Figure 9 shows the square of the acoustic pressure amplitude as a function of $\dot{Q}_h$. There is also a linear dependence between the two variables. Figure 10 shows ΔT as a function of $\dot{Q}_h$. ΔT has a minimum value of approximately 321 K, at a heat input of approximately 70 W. This minimum is taken to be the ΔT_{onset}. This value is indicated in Fig. 4 by the " * " symbol. The DeltaE result is in good agreement with both the measured result and the result of the MATLAB program.

A similar procedure (see Figs. 11- 13) yields a ΔT_{onset} of approximately 341 K for a mean gas pressure of 500 kPa. This result is indicated on Fig. 5 by the " * " symbol. This value is also in good agreement with the measured predicted results. Detailed input files for DeltaE are given in Appendix A and B.

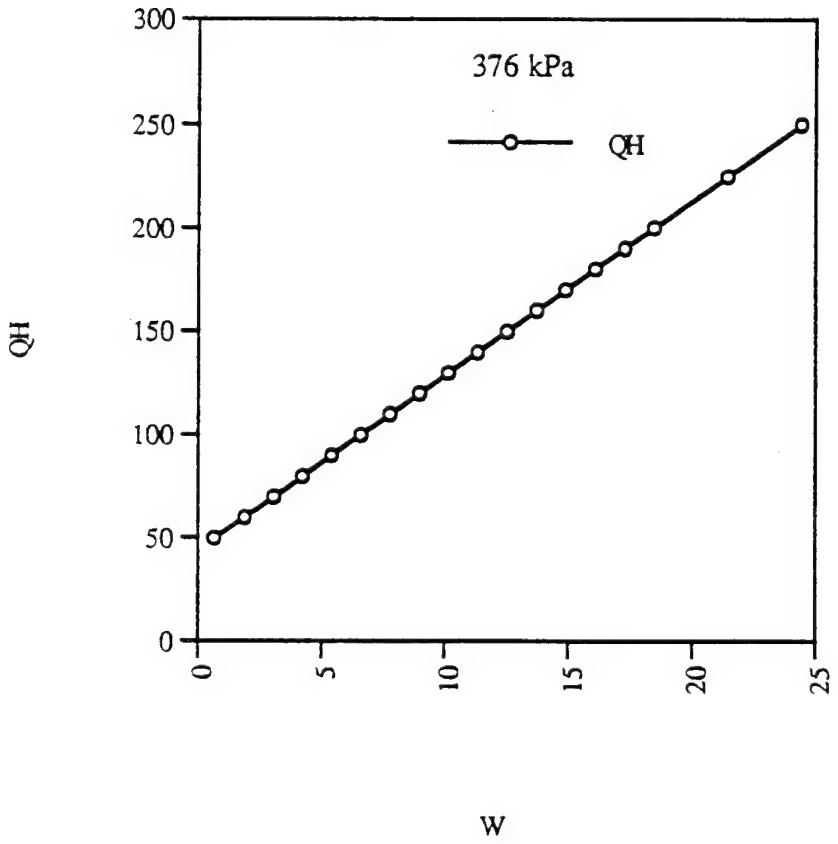

Figure 8 - Graph of heat input vs. work output for Lin's prime mover filled with helium gas . The results are from DeltaE. The mean gas pressure is 376 kPa.

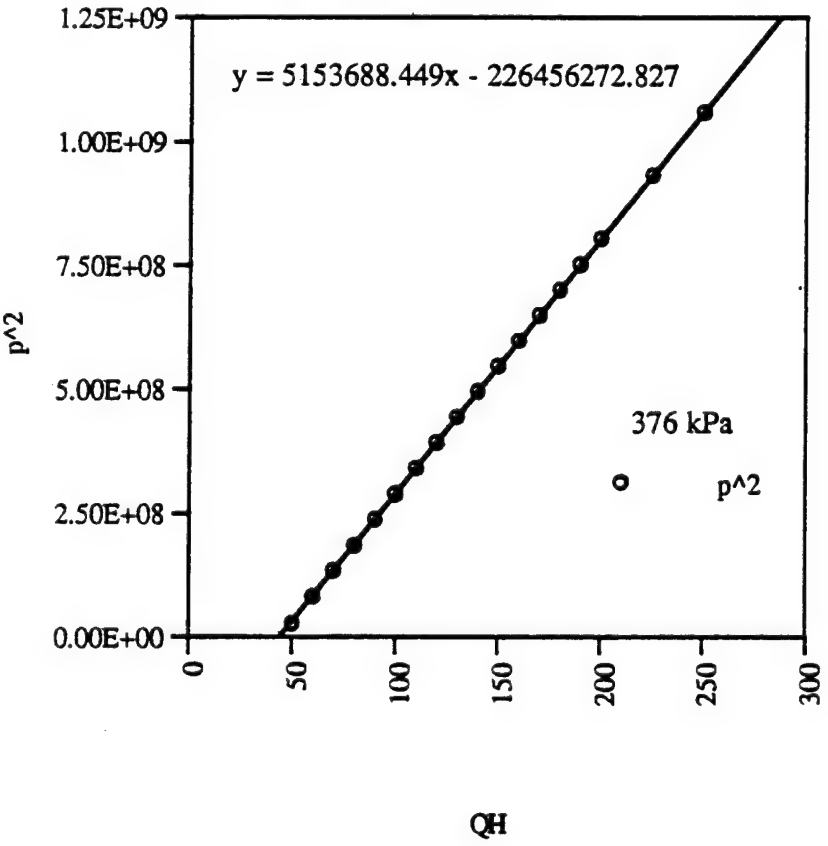

Figure 9 - Graph of the square of the acoustic pressure amplitude vs. heat input for Lin's prime mover filled with helium gas. The results are from DeltaE. The mean gas pressure is 376 kPa.

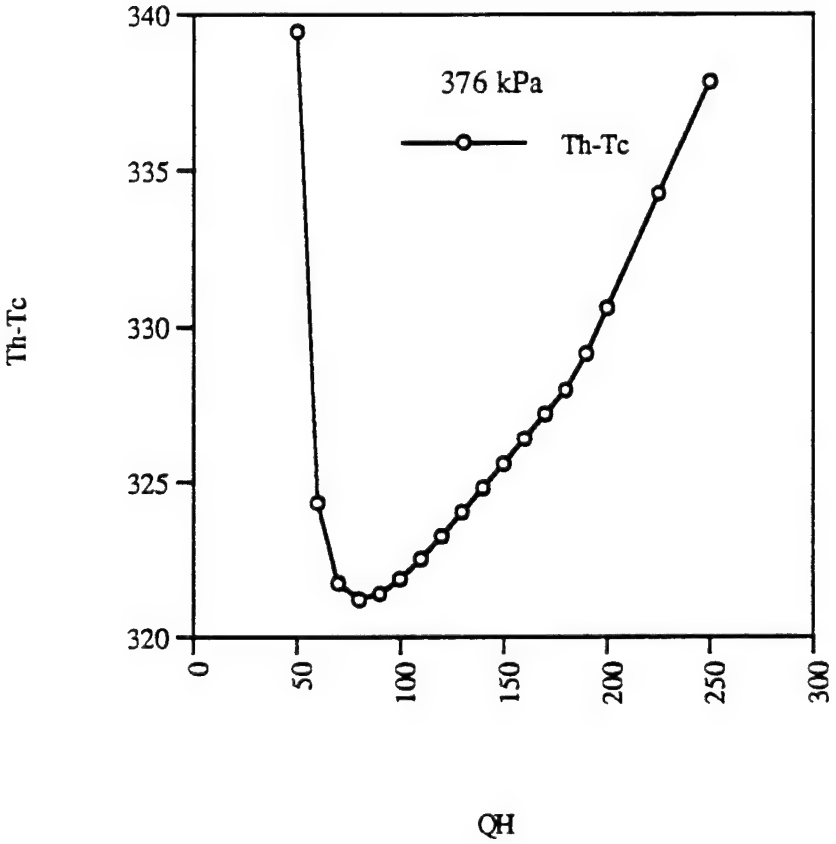

Figure 10 - Graph of ΔT vs. heat input for Lin's prime mover filled with helium gas. The results are from DeltaE. The gas pressure is 376 kPa

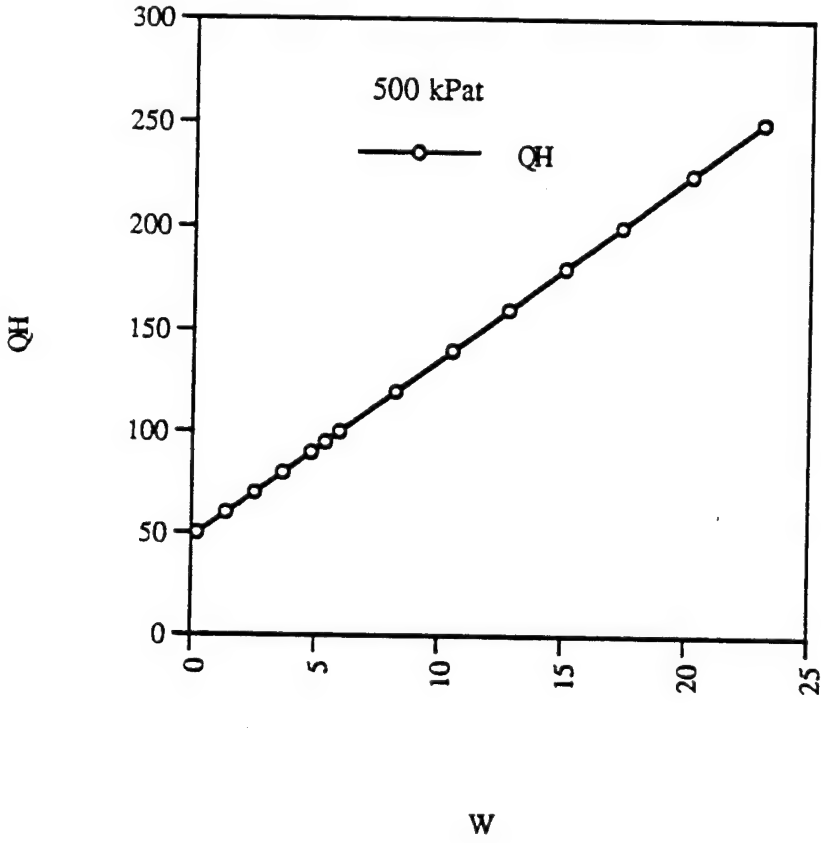

Figure 11 - Graph of heat input vs. work output for Lin's prime mover filled with helium gas. The results are from DeltaE. The mean gas pressure is 500 kPa.

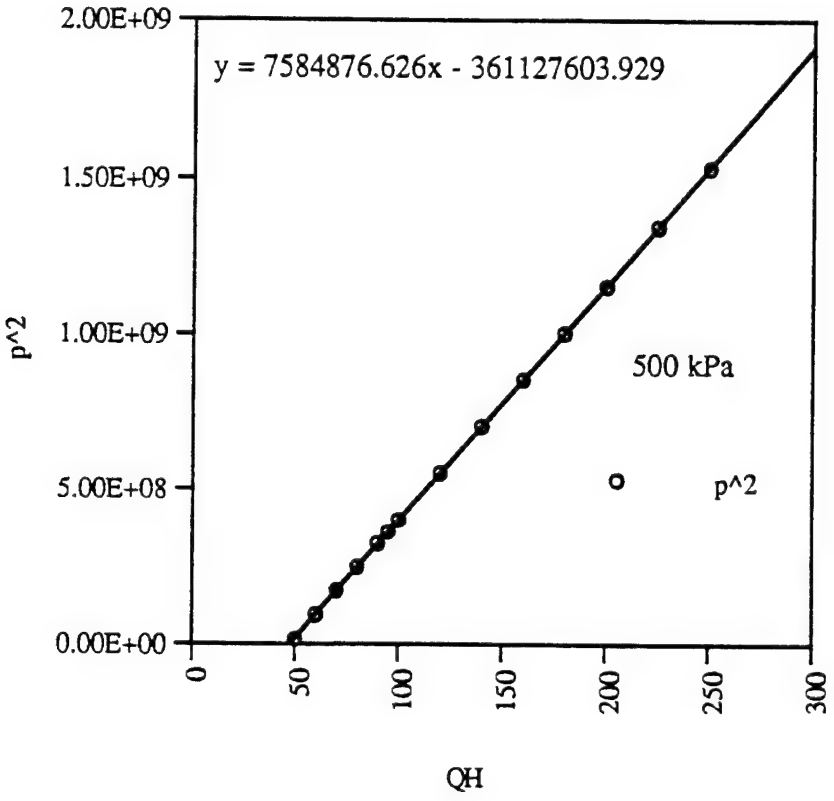

Figure 12 - Graph of the square of the acoustic pressure amplitude vs. heat input for Lin's prime mover filled with helium gas The results are from DeltaE. The mean gas pressure is 500 kPa

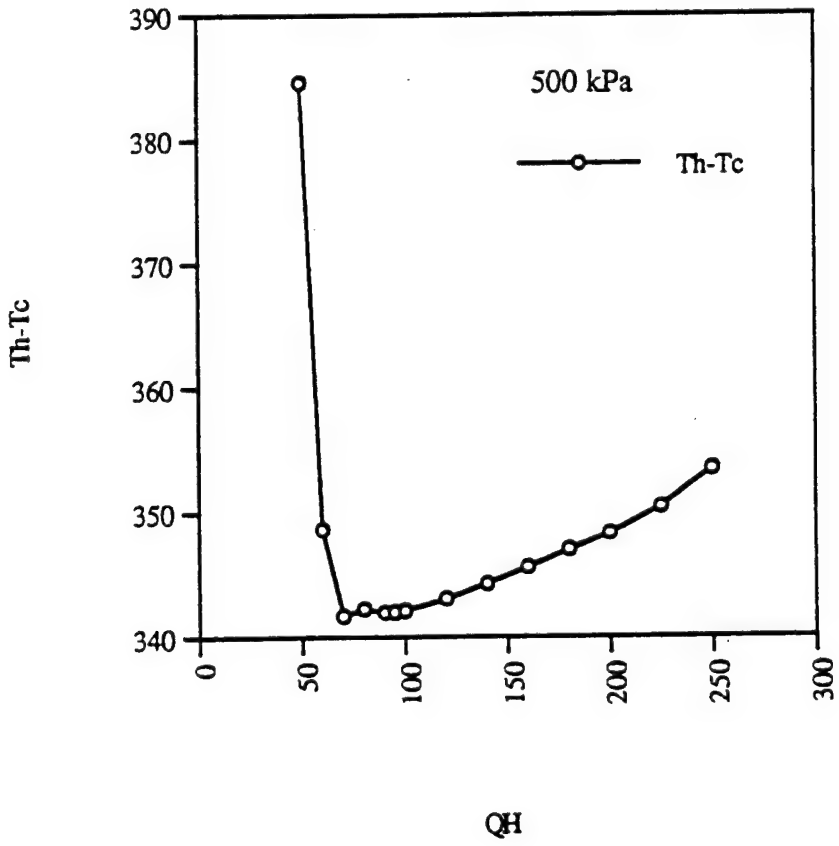

Figure 13 - Graph of ΔT vs. heat input for Lin's prime mover filled with helium gas. The results are from DeltaE. the gas pressure is 500 kPa.

IV. TOROIDAL PRIME MOVER

Having demonstrated the ability to predict the onset conditions for Lin's prime mover with the MATLAB program, the next step is to analyze a toroidal prime mover. One possible configuration is shown in Fig. 14. Heat is supplied to the hot heat exchanger and heat is removed from the cold heat exchanger, forcing a temperature gradient across the stack as usual. A rigid-ended prime mover would simply have rigidly-capped hot and cold (isothermal) ducts attached to the heat exchanger. However, in the toroidal geometry the hot and cold ducts are connected together, resulting in a temperature discontinuity at the junction. Of course, this discontinuity would be smoothed out by thermal conduction, so that there would be a gradual, continuous temperature change along the duct. This gradient will have some thermoacoustic effect that must be taken into account. More importantly, if the duct has a non-negligible thermal conductivity, a significant amount of heat will be conducted through it, perhaps requiring an excessive heat input to reach onset.

To avoid the detrimental conduction through the duct, a toroidal prime mover might have two insulator sections, one attached to each of the hot and cold heat exchangers. The use of insulators will allow the duct to be held at ambient temperature while at the same time having little conduction through it. The disadvantage of the insulators is that the temperature gradient across them can be high. However, since the surface area is much smaller than that of the stack, any thermoacoustic effect will be small.

Due to unfortunate time constraints, attemps to build a toroidal prime mover were limited to off-the-shelf components and those already on hand. This combination resulted in a compromised design. These compromises were understood from the outset, yet it was decided to complete the construction as a learning step toward a functioning toroidal prime mover.

This chapter contains a description of the toroidal prime mover, analysis of the prime mover based on the MATLAB program, and a description of measurements performed, along with the results.

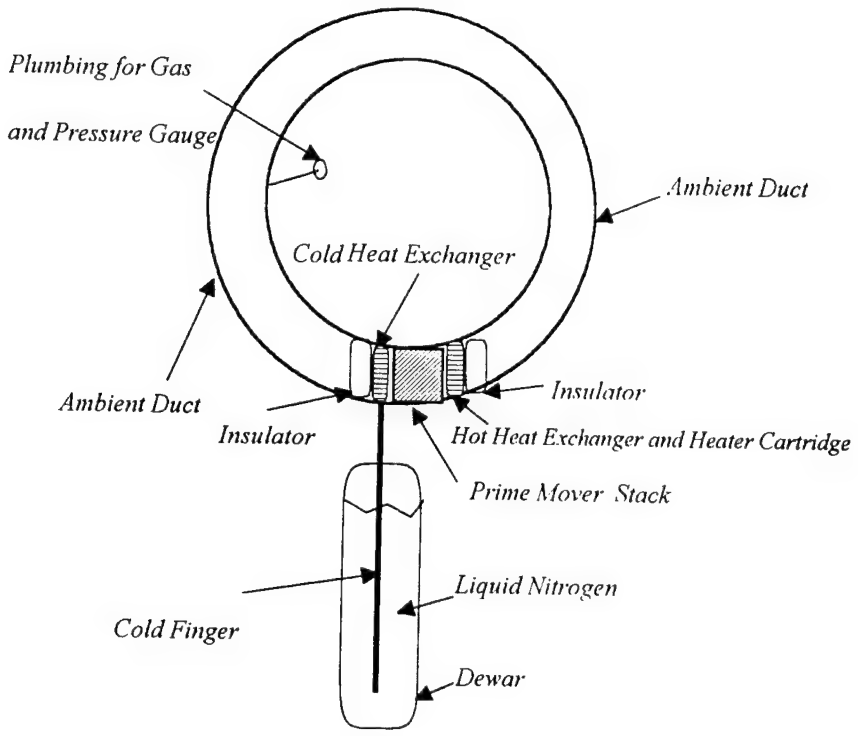

Figure 14 - Toroidal Prime Mover Configuration

A. TOROIDAL PRIME MOVER DESIGN

Figure 14 shows an illustration of the toroidal prime mover. This section contains specific details. The hot and cold heat exchangers and the stack and stack holder are those used by Castro [Ref. 2]. More complete details can be found there.

1. Ambient Duct Assembly

The ambient duct assembly is made from four sections of bent, galvanized steel conduit. Each section is 4.4 cm O.D., 4 cm I.D., and 48 cm long. The tubes are joined together with 2.35 cm long brass collars and soldered.

2. Insulator

The stainless steel insulators are sections of tube, 4 cm long, 3.85 cm I.D. and 4.0 cm O.D. They are located between the ambient duct assembly and hot and cold heat exchangers to reduce heat conduction to the duct. The stainless steel tube is soldered to two stainless steel flanges. One flange is bolted to the ambient duct, the other to the heat exchanger and stack holder.

3.Hot Heat Exchanger Assembly

The assembly consists of hot heat exchanger, hot heat exchanger holder and hot heat exchanger heater collar. The copper heat exchanger is 3.924 cm in diameter and 0.257 cm thick. Each plate within the heat exchanger is 0.0292 cm thick. The plate gap is 0.0584 cm. The heat exchangers are soldered into the heat exchanger holder. The copper heat exchanger holder is 7.366 cm O.D. and 0.953 cm thick. There is an O-ring groove in the side facing the stack.

The hot heat exchanger heater collar is made of 0.953 cm thick copper and bolted around the hot heat exchanger holder. The collar is roughly square in cross section, 8.2 cm long on edge. It has a 7.37 cm I.D. hole cut in it to fit over the heat exchanger holder. The collar is split and bolted together around the holder. There are two 0.625 cm diameter holes drilled in each piece to hold two heater cartridges, used to maintain a constant hot heat exchanger temperature.

4.Stack Assembly

The prime mover stack assembly consists of the stack and the stack holder. The stack is made of 0.01 cm thick polyester film. The film is rolled spirally around a phenolic

core 0.635 cm in diameter and 2.529 cm long. The polyester film is separated by 0.851 mm diameter fishing line. The stack is 2.553 cm long, 3.772 cm O.D. and has a total surface area of 583 cm^2.

The 304 stainless steel stack holder is 2.576 cm long and 3.772 cm I.D. (The stack holder is 0.22 mm longer than the stack creating a 0.11 mm gap on each side of the stack inside the holder). The stack holder has eight 8-32 machine screw holes in each flange to attach the insulator and hot heat exchanger on one side and the cold heat exchanger and insulator on the other.

5.Cold Heat Exchanger Assembly

The assembly consists of cold heat exchanger, cold heat exchanger holder and cold finger. In order to impose a temperature gradient across the stack, a 65.5 cm long, 0.7 cm thick, 10 cm wide copper plate (or cold finger) is bolted around the cold heat exchanger holder and immersed in liquid nitrogen. The cold heat exchanger assembly is similar to the hot heat exchanger assembly, except that the cold heat exchanger holder has no O-ring groove. The cold heat exchanger is sealed by using a 0.03 cm thick teflon gasket in the stack side of the cold heat exchanger holder and a 0.17 cm diameter lead wire diameter gasket on the insulator side.

B. MATLAB PROGRAM SIMULATION

In order to determine the best operating mean pressure, resulting in the lowest ΔT_{onset}, the toroidal prime mover has modeled with the MATLAB program. As was mentioned earlier, designing a functioning toroidal prime mover is considerably more difficult than designing a conventional prime mover. For example, in a conventional prime mover, placement of a rigid boundary in the engine insures that the acoustic velocity is zero at that point. These boundary conditions serve as a convenient starting point for computational analysis of the performance of an engine. Unlike the conventional prime mover, the toroidal prime mover has no rigid boundary. Therefore, the location of the stack relative to the nearest pressure antinode is an adjustable parameter.

Figure 15 shows a 3-D plot of ΔT_{onset} versus mean gas pressure of neon and x_s, where x_s is the distance from the location of the assumed pressure antinode to the hot end of the stack. The shape of the surface indicates the general dependence of ΔT_{onset} on those two variables. It is seen that the value of x_s yielding the lowest ΔT_{onset} is 21 cm.

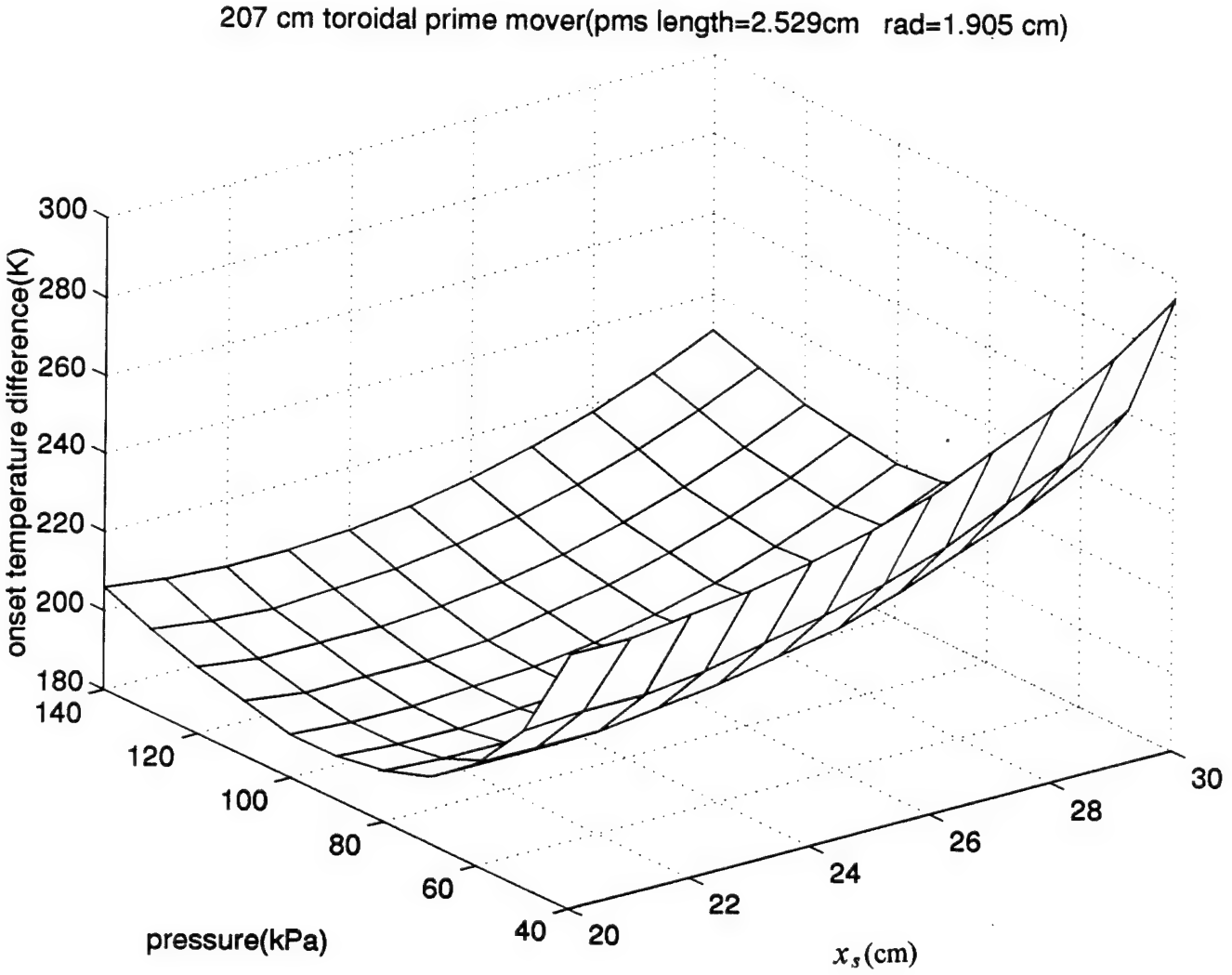

Figure 15 - Graph of ΔT_{onset} vs. mean pressure and stack location.

Figure 16 shows ΔT_{onset} versus mean gas pressure for x_s =21 cm. It is seen that the lowest value of ΔT_{onset} is approximately 190 K at a pressure of 100 kPa. Acknowledging the tendency of the program to under predict ΔT_{onset}, a reasonable value for ΔT_{onset} is approximately 190-210 K. The largest possible ΔT attainable with liquid nitrogen and a hot end at nominal room temperature is approximately 220 K. Therefore, it is seen that the expected onset conditions are right at the limits of what is easily achieved.

C. EXPERIMENTAL PROCEDURE

The toroidal prime mover was pumped down using a vacumn pump to approximately 10 kPa and filled back with neon to approximately 100 kPa. This procedure is performed three times to ensure the gas inside the prime mover is substantially pure neon. Next, the dewar was filled with liquid nitrogen, cooling the cold heat exchanger. As the cold heat exchanger cooled down, heat was supplied to the hot heat exchanger via the heater cartridges to maintain the hot end temperature at approximately 293 K. The cold heat exchanger was surrounded by thermal insulation to reduce the heat leak to the surroundings. The temperature of the cold heat exchanger was measured with a type J thermocouple clamped between the cold heat exchanger holder and the cold finger collar. The coldest temperature achieved was approximately 110 K.

Temperature control of the hot heat exchanger is achieved by a digital temperature controller (Omega CN 9000 temperature controller), heater cartridges, and a power supply amplifier (Techron 5530 power supply amplifier). The reference temperature for the temperature controller is taken from a type J thermocouple placed between the hot heat exchanger holder and the heater collar. The controller sends a 10 volt DC pulse to the mono input in the power supply amplifier. The duty cycle of the phase is proportional to the difference between the set point temperature and the thermocouple reading. Power to the heater catridges is provided by the output of the power supply amplifier. The hot end temperature was maintained to within approximately ±5 K of the set point temperature, initially 293 K.

The pressure inside the toroidal prime mover is measured with a piezoresistive transducer with a sensitivity of 17.05 mv/psi. The transducer is mounted in the wall of the ambient duct, approximately 40 cm from the hot end of the stack. The transducer measures the mean pressure as a DC signal and the acoustic pressure amplitude as an AC

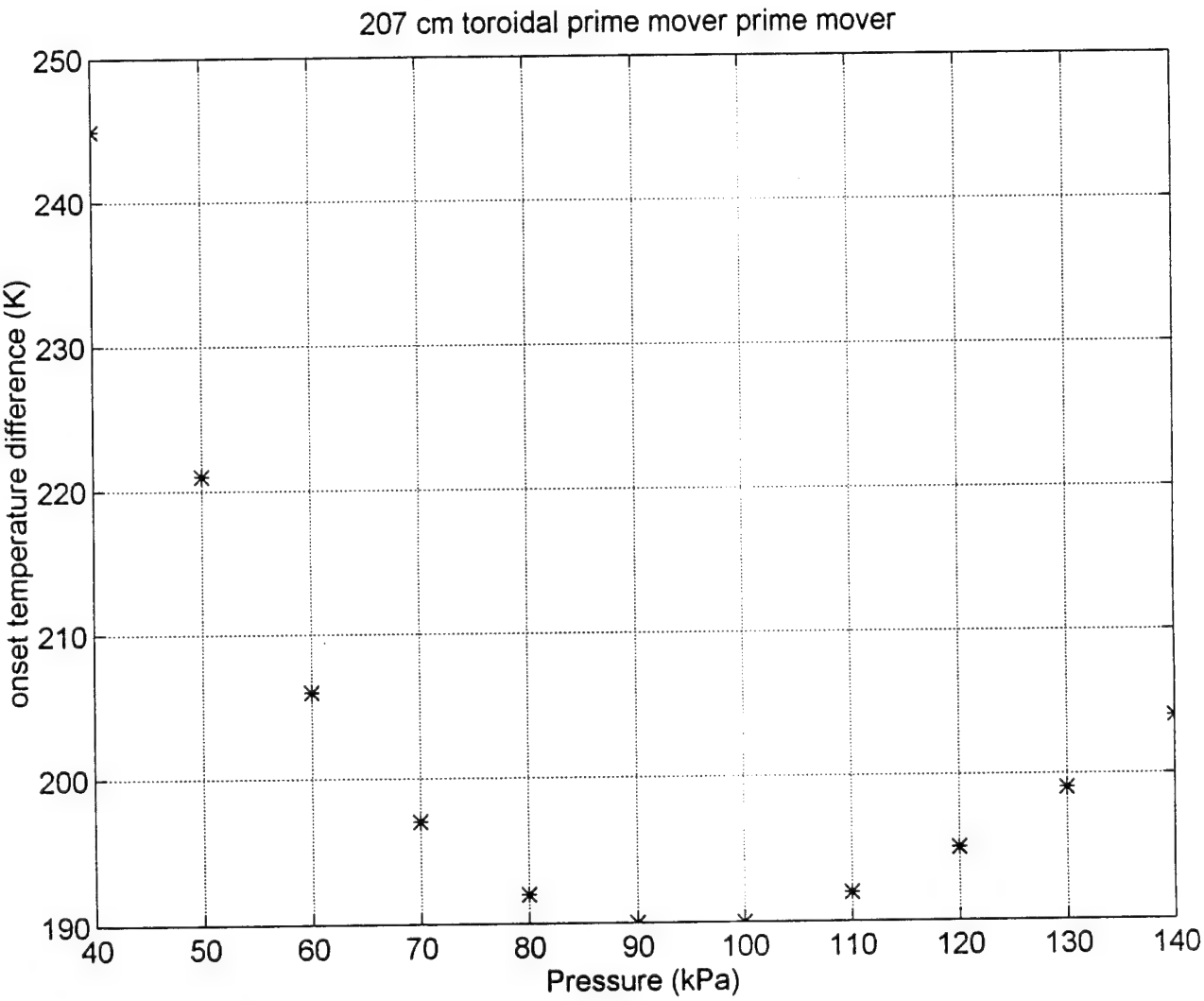

Figure 16 - Graph of ΔT_{onset} vs. mean pressure of neon gas for $x_s = 21$ cm as predicted with the MATLAB program.

signal, simultaneously. The transducer output is sent to a DC coupled preamplifier with a gain of 10.

D. EXPERIMENTAL RESULTS

The toroidal prime mover failed to reach onset at a mean pressure of 100 kPa and a ΔT of approximately 180 K (cold end temperature = 110 K, hot end temperature =293 K). At this point the hot end temperature was increased to approximately 330 K, and the mean pressure varied over a range from approximately 20 kPa to 140 kPa. The prime mover still failed to go into onset.

There are two possible explanations: 1) The applied ΔT was not large enough, or 2) The prime mover would never go into onset for reasons discussed earlier dealing with how the stack might influence the orientation of the standing wave.

The null result suggests two possible paths for further study. 1) Design a prime mover with a lower ΔT_{onset}. This path is the subject of Chapter V. 2) Modify the existing toroidal prime mover to make it go into onset, to test the computer model.

It was decided to remove approximately half the ambient duct from the toroidal prime mover and rigidly cap the remaining sections. This operation converted the toroid to a half-toroid. The new prime mover configuration is similar to a conventional prime mover except for the insulator sections and the two end ducts having the same temperature.

The duct was cut and capped such that the hot end of the stack was 20 cm from the rigid end. The total length of the half-toroid was 108 cm. Figure 17 shows the output of the MATLAB program for the half-toroid configuration. The predicted ΔT_{onset} is approximately 117 K at a mean pressure of 100 kPa.

The prime mover was filled with neon gas to a pressure of 100 kPa and the cold end was cooled down with liquid nitrogen, as explained previously. Onset was observed at a ΔT of approximately 110 K. This measured result agrees with the predicted value to within 7 K. The agreement gives some indication of how much the prediction for the whole-toroid might be in error.

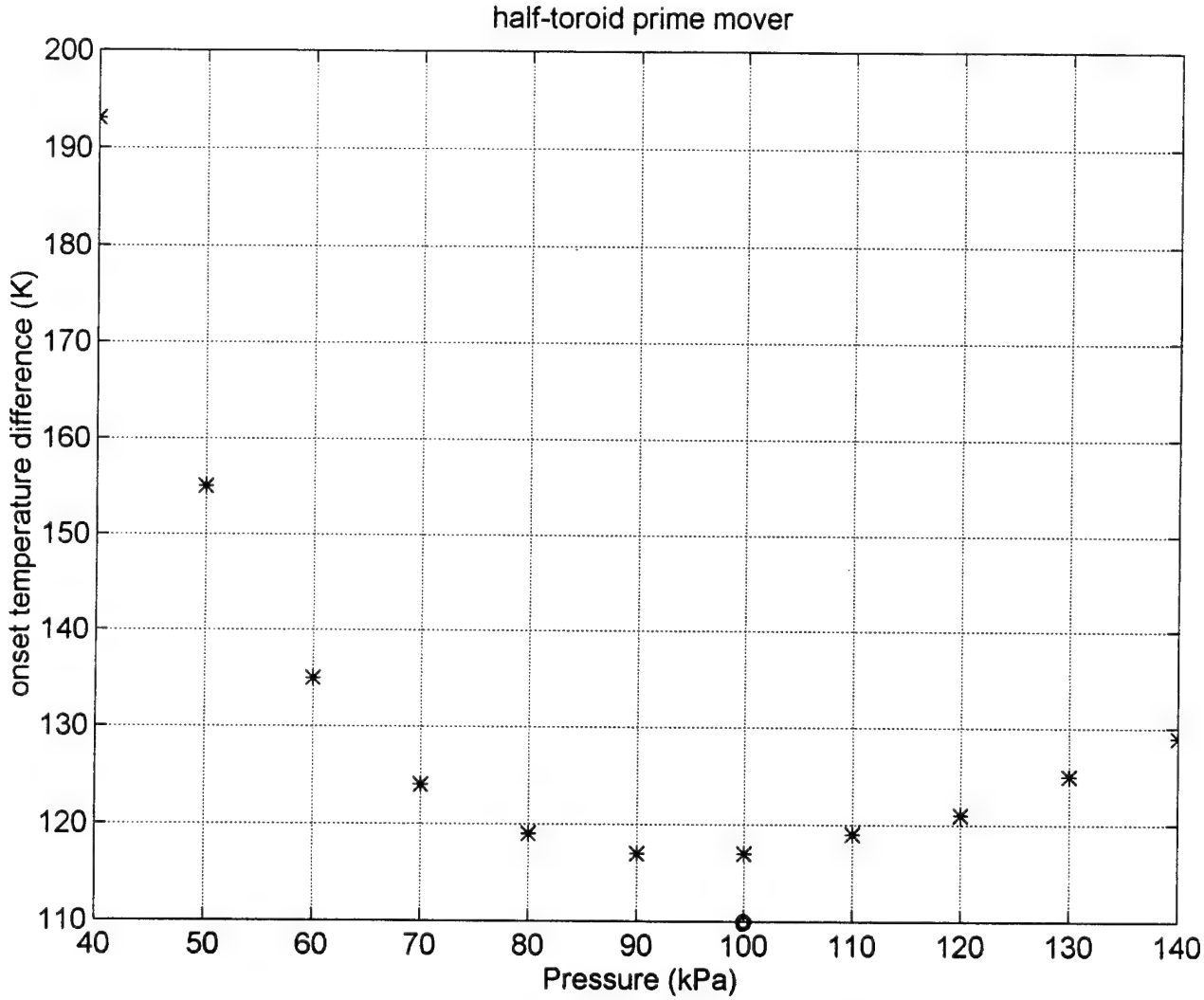

Figure 17 - Graph of ΔT_{onset} vs. mean pressure of neon gas for the half-toroid prime mover as predicted with the MATLAB program. The "o" represents the measured onset point.

V. IMPROVED DESIGN

A. OPTIMIZING PARAMETERS

The null result of the attempt to reach onset with the toroidal prime mover discussed in Chapter IV, leaves the basic question "Will a toroidal prime mover work?" unanswered. One obvious step is to redesign the prime mover to lower its predicted ΔT_{onset} to a value easily attainable. This redesign is the topic of this chapter.

In considering the design, it was decided to assume the same stack and heat exchanger plate spacing as described in Chapter IV. The heat exchanger length is also the same. Three parameters were investigated: 1) the length of the stack, 2) the radius of the duct, and 3) the circumference of the toroid. It should be pointed out that ΔT_{onset} for some of the parameters shown exceeds 216 K (the value of ΔT possible between nominal room temperature, 293 K, and liquid nitrogen temperature, 77 K). Therefore, for these plots we have set the hot heat exchanger temperature equal to 373 K. The temperature of the ambient duct is is 293 K. Thus, there is a 100 K temperature difference across the hot end insulator. This temperature difference is in the wrong direction, thermoacoustically. This will tend to make the predicted ΔT_{onset} higher than might be expected. Also, the thermophysical parameters of the gas will be somewhat different. However, these considerations do not significantly alter the conclusions draw from the results.

Figure 18 shows the effect of changing the length of the stack. The graph shows ΔT_{onset} versus mean pressure of neon for x_s = 21 cm. The symbols are for three different stack lengths: 3.175 cm, 2.529 cm, and 1.905 cm. The circumference is 207 cm. It is seen that the shorter stack gives the lowest value of ΔT_{onset}. There are two reasons for this result. First, for a fixed ΔT, a shorter stack results in a larger temperature gradient. Also, the shorter stack has less viscous loss.

Figure 19 shows the effect of changing the radius of the prime mover. Again, the graph shows ΔT_{onset} versus gas pressure at x_s = 21cm and a 1.905 cm long stack. Three different radii are shown: 2.54 cm, 1.905 cm, and 1.27 cm. The lowest ΔT_{onset} is occurs for the largest radius and is approximately 133 K. The reason for the decrease with increasing radius is that 1/Q is proportional to the ratio of the volume of gas contributing to losses to the volume of gas storing energy. This ratio is roughly proportional to δ/R.

Finally, the effect of changing the circumference is investigated. As discussed in Chapter I, any nonuniformities in the cross section of the toroid may affect the spatial

orientation of the standing wave. Therefore, it is important to have as nearly a uniform cross section as possible. One way to make a uniform cross section is to machine a toroid out of a single piece of stock. A 207 cm circumference is perhaps too large to do this easily. Therefore, the effect of decreasing the circumference was investigated. In decreasing the circumference from 207 cm to 150 cm, the resonance frequency increases. Therefore, the position of the stack relative to the standing wave changes. In order to keep the stack at the right place, the value of x_s must be decreased by a factor 150/207 to keep kx_s the same in the two cases. Therefore, x_s for the 150 cm circumference resonator is 15 cm. The results of this simple calculation are verified in Fig. 20 which is a 3-D plot for the150 cm prime mover. It is seen that the minimum value of ΔT_{onset} (152 K) occurs at x_s approximately equal to 15 cm. Figure 21 shows ΔT_{onset} versus gas pressure for a 1.905 cm long stack and 2.54 cm radius toroid. Two circumferences are shown: 207 cm and 150 cm. It is seen that decreasing the circumference increase ΔT_{onset} to approximately 152 K. It also decreases the optimum mean pressure to approximately 70 kPa. Decreasing the circumference more increases ΔT_{onset} further. The 150 cm circumference is a reasonable compromise between the need for a low ΔT_{onset} and having a prime mover size small enough for machining that is easily from a single piece of stock.

B. SUMMARY

The main finding of this thesis is a preliminary design of a toroidal prime mover. The results of a first-step design indicates that a useful geometry has a 1.9 cm long stack and 2.5 cm radius. ΔT_{onset} for this configuration is predicted to be approximately 150 K at 70 kPa mean pressure of neon.

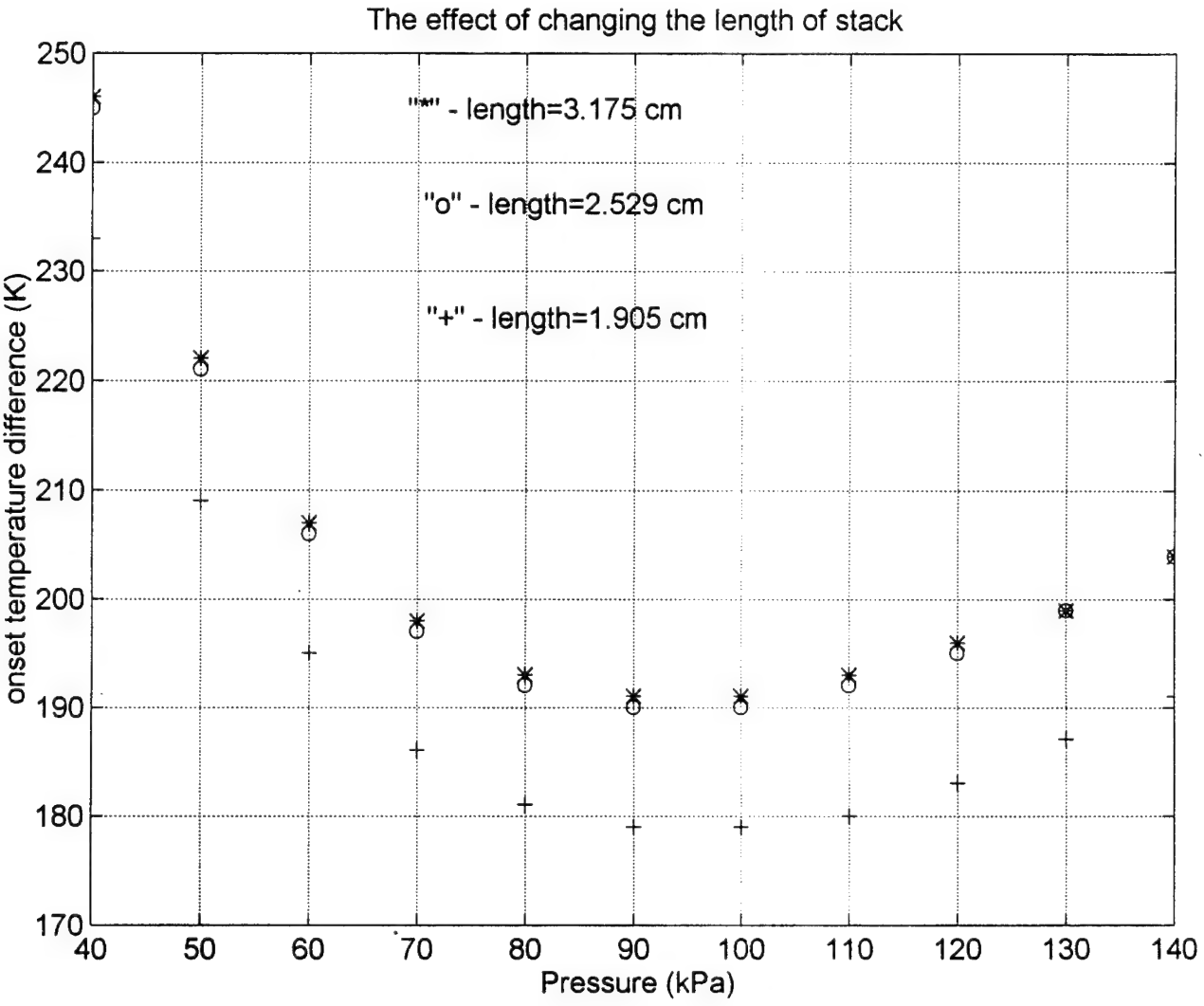

Figure 18 - Graph of ΔT_{onset} vs. mean gas pressure for the toroidal prime mover for three stack lengths.

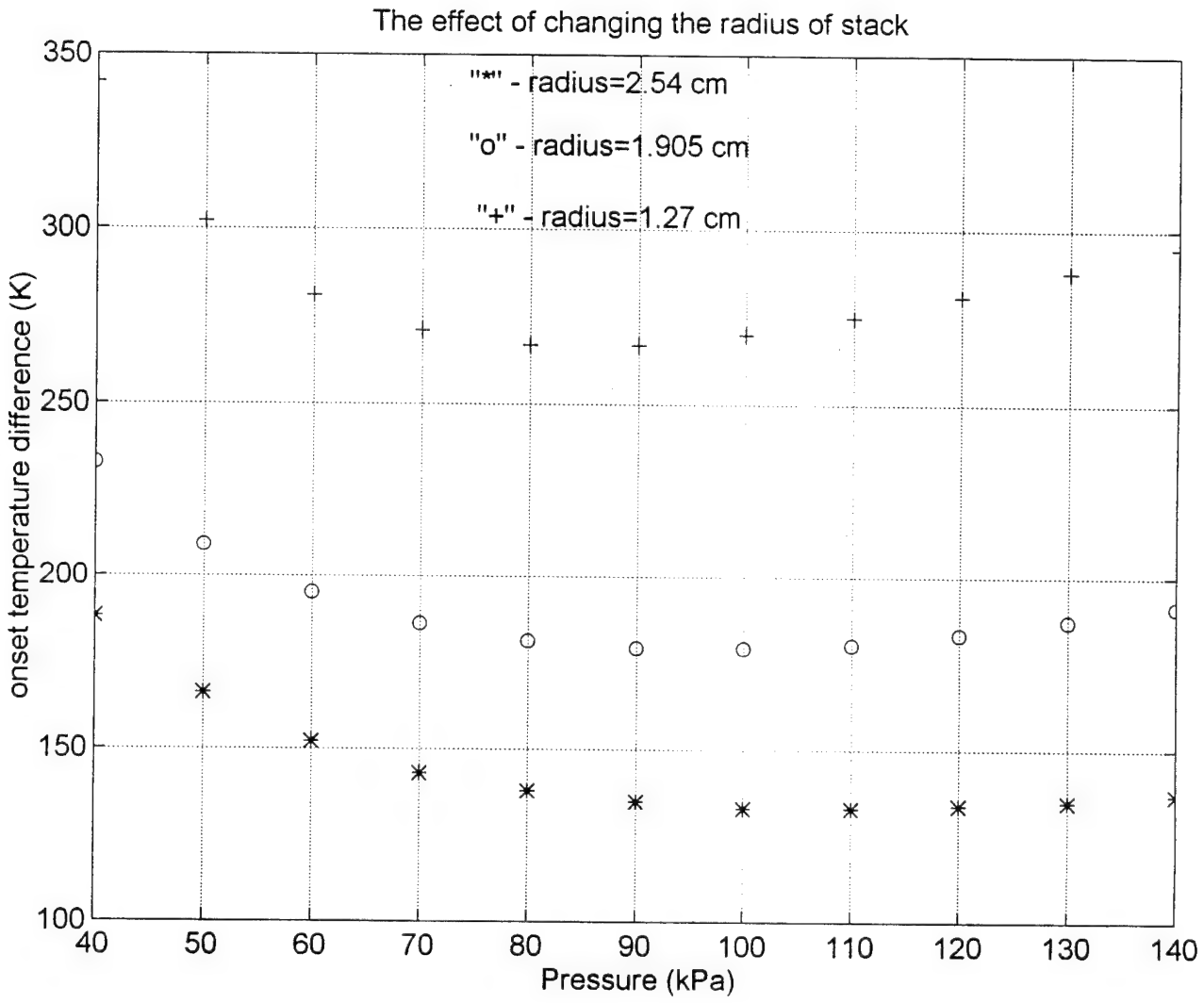

Figure 19 - Graph of ΔT_{onset} vs. mean gas pressure for the toroidal prime mover for three different duct radii.

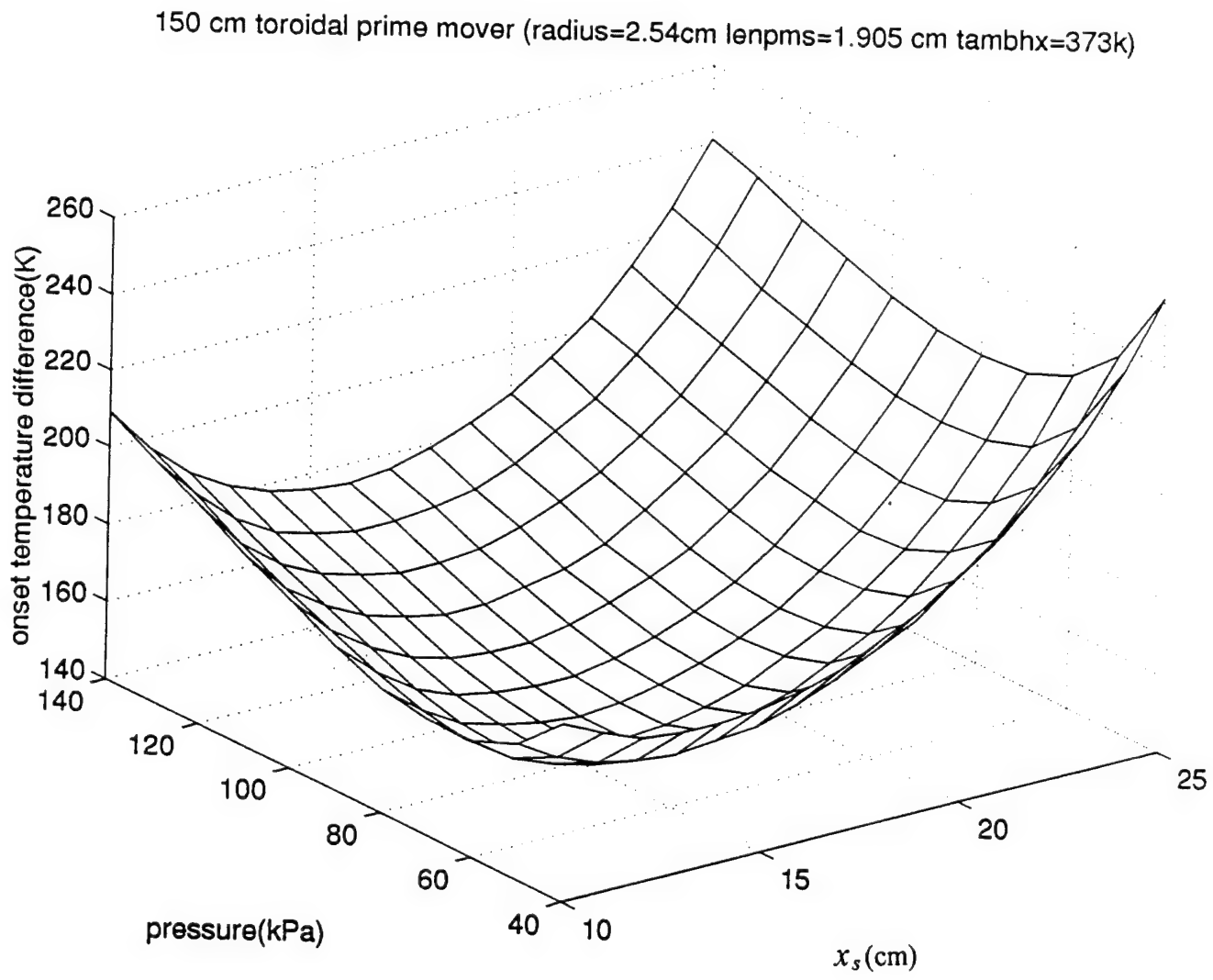

Figure 20 - 3-D plot for the 150 cm toroidal prime mover

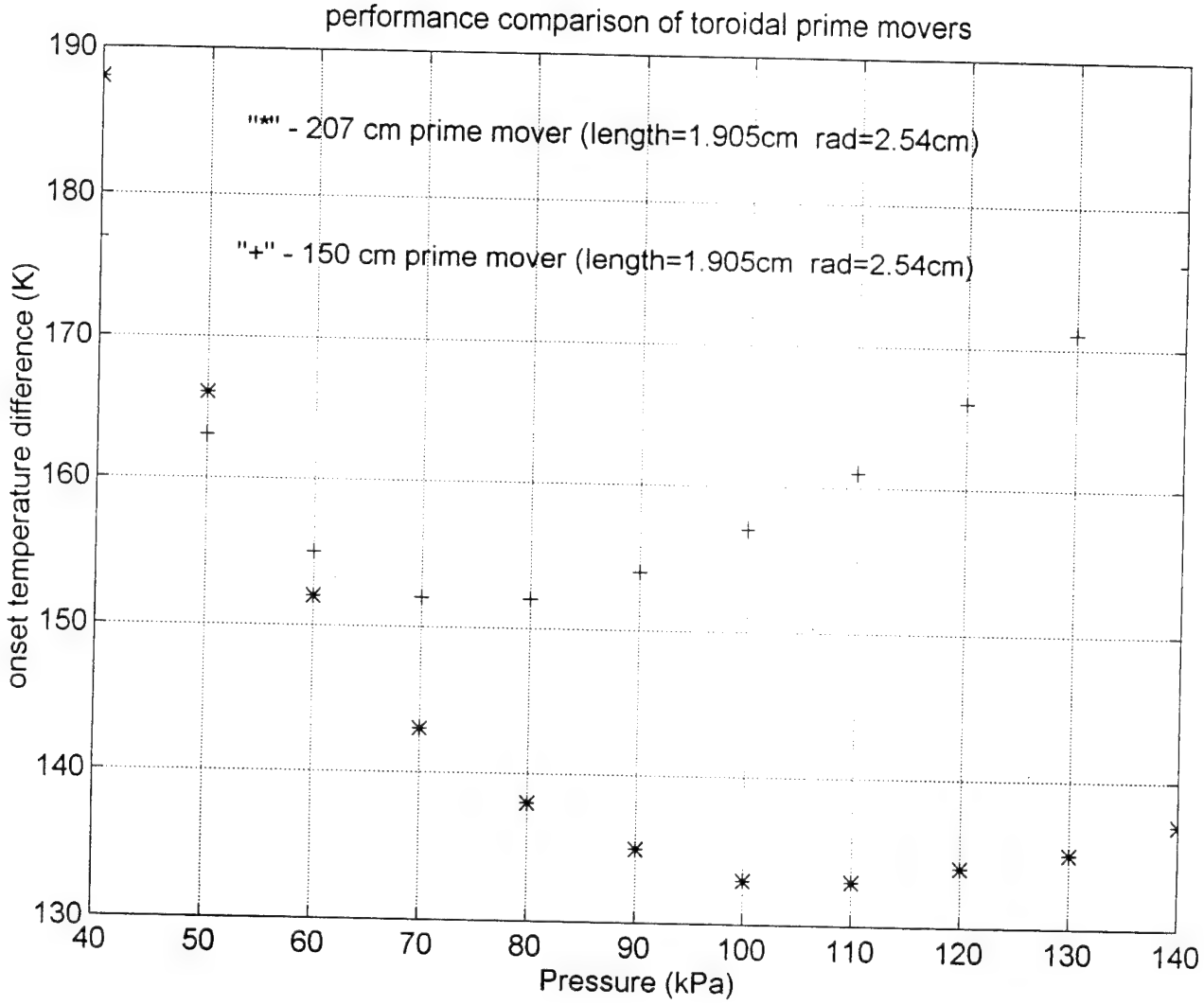

Figure 21 - Graph of ΔT_{onset} vs. mean gas pressure for the toroidal prime movers for two different circumferences.

APPENDIX A. INPUT FILE FOR LIN'S PRIME MOVER

```
TITLE  Lin's Thermoacoustic Prime Mover Input File
BEGIN     Initial          0
 3.76E+05 a Mean P    Pa
  591.    b Freq.    Hz    G
  400     c T-beg    K
 3.76E+04 d |p|@0     Pa    G
 0.000    e Ph(p)0    deg
 0.000    f |U|@0     m^3/s
 0.000    g Ph(U)0    deg
helium    Gas type
copper    Solid type

ENDCAP    Hot End          1
 1.146E-03 a Area     m^2
sameas  0  Gas type
copper    Solid type

ISODUCT   Hot Duct         2
sameas  1a  a Area     m^2
 0.12    b Perim     m
 0.055   c Length    m

sameas  0  Gas type
copper    Solid type

HXFRST    Hot HX           3
sameas  1a  a Area     m^2
 0.697 b GasA/A
 7.620E-03 c Length    m
 5.200E-04 d y0        m
 250.0   e HeatIn    W
 500.0   f Est-T     K    (t)
sameas  0  Gas type
nickel    Solid type

STKSLAB   Prime Mover Stack      4
sameas  1a  a Area     m^2
 0.733 b GasA/A
```

```
3.500E-02 c Length     m
 3.850E-04 d y0        m
 1.400E-04 e Lplate    m
helium    Gas type
stainless  Solid type

HXLAST    Ambient HX          5
 sameas  1a  a Area    m^2
 0.697   b GasA/A
 2.040E-02 c Length    m
 5.2E-04 d y0        m
 0.000    e HeatIn    W    (t)
  293.    f Est-T     K    (t)
helium    Gas type
copper     Solid type

ISODUCT   Cold Duct          6
sameas  5a  a Area     m^2
 0.12    b Perim     m
 0.8795    c Length    m
helium    Gas type
ideal     Solid type

ENDCAP    Cold End          7
sameas  5a  a Area     m^2
helium    Gas type
copper     Solid type

HARDEND   8                 8
 0.000    a R(1/Z)
 0.000    b I(1/Z)
helium    Gas type
copper    Solid type
```

APPENDIX B. INPUT FILE FOR LIN'S PRIME MOVER

```
TITLE  Lin's Thermoacoustic Prime Mover Input File
BEGIN     Initial          0
 5E+05 a Mean P   Pa
  591.   b Freq.   Hz    G
  400    c T-beg   K
 5E+04 d |p|@0    Pa    G
 0.000    e Ph(p)0   deg
 0.000    f |U|@0    m^3/s
 0.000    g Ph(U)0   deg
helium    Gas type
copper    Solid type

ENDCAP    Hot End          1
 1.146E-03 a Area     m^2
sameas  0  Gas type
copper    Solid type

ISODUCT   Hot Duct         2
sameas  1a  a Area     m^2
 0.12    b Perim     m
 0.055    c Length    m

sameas  0  Gas type
copper    Solid type

HXFRST    Hot HX           3
sameas  1a  a Area     m^2
 0.697 b GasA/A
 7.620E-03 c Length    m
 5.200E-04 d y0        m
 250.0    e HeatIn    W
 500.0  f Est-T    K    (t)
sameas  0  Gas type
nickel    Solid type

STKSLAB   Prime Mover Stack      4
sameas  1a  a Area     m^2
 0.733 b GasA/A
```

```
3.500E-02 c Length     m
 3.850E-04 d y0        m
 1.400E-04 e Lplate    m
helium    Gas type
stainless  Solid type

HXLAST    Ambient HX          5
 sameas  1a  a Area    m^2
 0.697   b GasA/A
 2.040E-02 c Length    m
 5.2E-04 d y0        m
 0.000    e HeatIn    W    (t)
  293.    f Est-T     K    (t)
helium    Gas type
copper     Solid type

ISODUCT   Cold Duct          6
sameas  5a  a Area     m^2
 0.12    b Perim     m
 0.8795    c Length    m
helium    Gas type
ideal     Solid type

ENDCAP    Cold End          7
sameas  5a  a Area     m^2
helium    Gas type
copper     Solid type

HARDEND   8                 8
 0.000    a R(1/Z)
 0.000    b I(1/Z)
helium    Gas type
copper    Solid type
```

LIST OF REFERENCES

1. Hsiao-Tseng,Lin, "Investigation of a Heat Driven Thermoacoustic Prime Mover," Master's Thesis, Naval Postgraduate School, Monterey, CA, December 1989.

2. Nelson C. Castro, "Experimental Heat Exchanger Performance In a Thermoacoustic Prime Mover," Master's Thesis, Naval Postgraduate School, Monterey, CA, December 1995.

3. Fan-Ming, Kuo, "Stability Curves for a Thermoacoustic Prime Mover," Master's Thesis, Naval Postgraduate School, Monterey, CA, June 1993.

4. Anthony A. Atchley and Fan-Ming Kuo, "Stability Curves for a Thermoacoustic Prime Mover," J. Acoustic. Soc. Am. 95 (3), March 1994.

5. Anthony A. Atchley, "Standing Wave Analysis of a Thermoacoustic Prime Mover Below Onset of Self-Oscillation," J. Acoust. Soc. Am. 92 (5), November 1992.

6. MATLAB High-Performance Numeric Computation and Visualization Software Reference Guide, The Math Work Inc.

7. Ward, W., Swift, G.,Design Environment for Linear Thermoacoustic Engines DELTAE Tutorial and User's Guide, Los Alamos National Laboratory, July 1993.

8. Swift G. W.,"Thermoacoustic Engines," J. Acoust. Soc. Am., vol. 84, 1145-1180, 1988.

INITIAL DISTRIBUTION LIST

1. Defense Technical Information Center — 2
   Cameron Station
   Alexandria VA 22304-6145

2. Library Code 52 — 2
   Naval Postgraduate School
   Monterey CA 93943-5101

3. Prof. Anthony A. Atchley, Code PH/Ay — 3
   Department of Physics
   Naval Postgraduate School
   Monterey CA 93943-5000

4. Prof. Thomas J. Hofler, Code PH/Hf — 1
   Department of Physics
   Naval Postgraduate School
   Monterey CA 93943-5000

5. Library — 1
   Chinese Naval Academy
   P.O. Box 90175, Tso-Ying,
   Kao-Hsiung, Taiwan, R.O.C.

6. LCDR. Yang , Szu-Wei — 2
   #20 Tien-Tai St.
   Tao-Yuan, Taiwan, R.O.C.

7. Major Lin, Hsiao-Tseng — 1
   SGC # 2552, Naval Postgraduate School
   Monterey, CA, 93943

8. LCDR Meng, Ching-Kai — 1
   SGC # 2552, Naval Postgraduate School
   Monterey, CA, 93943